



The role of Dy2Sn2O7@Ar-C3N4/NFT nanoceramics in removing contaminants from refinery wastewater

Mostafa Khoshtabkh ¹, Mehdi Nobahari ¹*, Seyed Mojtaba Movahedifar ¹, Amin Honarbakhsh ¹, Rahele Zhiani ²

¹Department of Civil Engineering, Ne. C., Islamic Azad University, Neyshabur, Iran ² Department of Chemistry, Ne.C., Islamic Azad University, Neyshabur, Iran * E-mail: mehdinobahari@iau.ac.ir

Received 5 October 2025; accepted 16 November 2025

Abstract

The main objective of this study is to optimize the synthesis routes for producing high-performance nanoceramics and to systematically evaluate their efficiency in removing hazardous pollutants, including petroleum hydrocarbons, heavy metals, and recalcitrant organic compounds. In this work, a nanostructured Dy2Sn2O7@Ar-C3N4/NFT composite was successfully synthesized and characterized as an efficient photocatalyst for the purification of refinery wastewater. The synthesized nanoceramics were subjected to detailed structural, morphological, and functional characterization using X-ray diffraction (XRD), scanning electron microscopy (SEM), and Fourier transform infrared spectroscopy (FTIR). Moreover, the effects of key operating parameters such as pH, temperature, pollutant concentration, and catalyst dosage on photocatalytic efficiency were systematically investigated. The results demonstrated that the fibrous nanoceramic composite exhibits excellent photocatalytic activity and stability, leading to a remarkable reduction in various organic and inorganic contaminants. The optimized conditions significantly enhanced pollutant degradation rates, indicating promising potential for large-scale wastewater treatment applications. Overall, the study highlights the strong capability of Dy2Sn2O7@Ar-C3N4/NFT nanoceramics as a sustainable and efficient material for environmental remediation technologies.

Keywords: Fibrous nanoceramics, refinery wastewater treatment, industrial pollutants, filtration

1. Introduction

Refinery wastewater treatment is one of the most challenging environmental issues facing the petroleum industry. Traditional wastewater treatment methods, such as physical, chemical, and biological processes, are often ineffective in dealing with the complex and resistant to degradation compounds present in refinery wastewater. These methods may be expensive, produce excess sludge, or fail to completely remove contaminants. Therefore, the need to develop new and efficient technologies for treating these wastewaters is increasingly felt [1]. In recent years, panosorbents have been developed to

In recent years, nanosorbents have been developed to adsorb heavy metals, toxic compounds, radionuclides, organic and inorganic salts, bacteria and viruses in water and wastewater treatment systems. Advances in the synthesis of nanosorbents and their application in water and wastewater treatment systems have led to improved performance of the treated material and improved process operations. Increased system efficiency, reduced space requirements for treatment, and stable operation under various conditions are some of the advantages of using nanosorbents in water and wastewater treatment. Combining advanced nanotechnology with conventional treatment processes has provided a good prospect for the development of water and wastewater units [2].

Nanoceramics have emerged in recent years as one of the key materials for removing industrial wastewater pollutants, particularly in refineries. Complex composites such as Dy2Sn2O7@Ar-C3N4/NFT, with a dual oxidenitride structure, have demonstrated highly enhanced photocatalytic, adsorption, and thermal stability properties, making them an effective option for removing

both organic and inorganic contaminants from oilfield wastewater [3,4].

Oil refinery wastewater usually contains compounds such as phenols, sulfides, aromatic hydrocarbons, and heavy metals, which are serious threats to the environment. In this context, engineered nanostructures such as Dy2Sn2O7@Ar-C3N4/NFT with features such as high specific surface area, electron charge transport capability, and mesoporous structure can be highly effective in the photocatalytic adsorption and degradation of these compounds[5,6]. In addition to increasing the efficiency of pollutant removal, the use of Dy2Sn2O7@Ar-C3N4/NFT has advantages such as recyclability, high thermal and chemical stability, and favorable performance in weak light conditions, which distinguish it from older generations of nanomaterials. These advantages have led to such nanoceramics being recognized as potential substrates for use in advanced purification systems such as photoreactors and photoanodes [7].

Nasiri et al. (2025); used biohydrogels containing TiO₂ nanoparticles (as adsorbent and photocatalyst) and were able to increase the removal of oil and grease by up to 96% due to lipophilic/hydrophilic interactions with the gel structure. These gel structures are biodegradable and inexpensive and can act as effective pretreatment to reduce the surface load of refinery wastewater[8]. In a study conducted by Omrani et al. (2023), the removal of lead (II) ions from aqueous solutions using magnetic nanocomposites based on mesoporous silica was investigated. The results showed that under optimal conditions including a temperature of 80°C, an adsorbent dose of 0.04 g/L, pH 5.6, and a contact time of 38 minutes, the removal efficiency of lead (II) reached about 90%. Isotherm and kinetic analysis showed that the process followed the Langmuir model and pseudo-firstorder kinetic model well with R2 correlation coefficients of 0.98 and 0.99, respectively [9]. As a result, the research conducted shows that factors such as the type and concentration of materials, biomass composition, and the presence of accelerating or inhibiting materials have a great impact on the efficiency of biological treatment systems. Also, the use of different materials in treatment systems can help improve their performance and accelerate the process of pollutant removal at different scales [10].

2- Experimental method

2-1- Materials and Methods

High purity chemicals were obtained from Fluka and Merck. Field emission scanning electron microscopy (FESEM) images were recorded on a HITACHI Surface-4160S. FTIR spectra were recorded on a Bruker VERTEX. X-ray diffraction data were recorded on a Bruker Advanced 8D and Cuka radiation. The volume and pore diameter of the nanoparticles were determined by N2 absorption at 196°C using an ASAP Micromeritics

device. Pore size analysis was also performed on various instruments. A magnetic stirrer, Heater Stirrer, IKA, UK, was used for stirring. A laboratory oven, model UF119, made by Memmert, Germany, a K0012 electronic balance, and a centrifuge, model 48 MF CENTRIC, made by Domel, were also used.

2-2- Synthesis of NFT Nanoparticles

The synthesis process of NFT nanoparticles was initiated by adding 1.3 mL of tetrabutyl titanate to a mixture of cyclohexane and pentanol, of which 3.2 mL and 2.7 mL were used, respectively. Subsequently, a mixture of cetylpyridinium bromide and urea in deionized water was added to the solution, and the mixture was stirred for 24 minutes at ambient temperature.

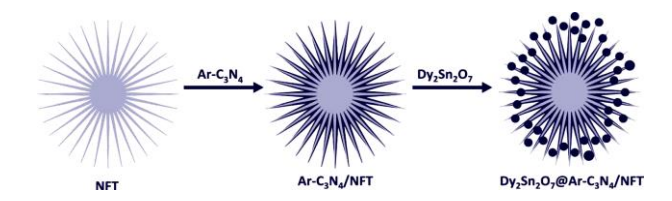


Figure 1 -Construction of the Dy2Sn2O7@Ar-C3N4/NFT

2-3- Synthesis of Ar-C₃N₄ (Ar = Pm, Py, Ph)

A mixture containing 0.6 g of dicyandiamide and 360 mg of 4-cyanopyridine was dissolved in 9 mL of methanol. The resulting solution was stirred for 1 hour at 60 °C. Afterwards, the solvent was removed using a low-pressure evaporator. To synthesize Pm-C₃N₄ and Ph-C₃N₄ nanosheets, pyrimidine-2-carbonitrile (360 mg) and terephthalonitrile (360 mg) were used as substitutes for 4-cyanopyridine (400 mg for Py-C₃N₄).

2-4- Synthesis of Ar-C₃N₄/NFT

Initially, a mixture of Ar-C₃N₄ (70 mmol) and NFT (2.3 mmol) was added to 26 mL of ethanol. The mixture was then refluxed under a nitrogen atmosphere for 18 hours. After methanol was removed under vacuum, the remaining solid was dissolved in deionized water and concentrated again under vacuum. The resulting mixture was subsequently separated using a combination of tetrahydrofuran and methanol.

2-5- Synthesis of Dy₂Sn₂O₇@Ar-C₃N₄/NFT

In this process, Dy(NO₃)₃•5H₂O (4 mmol) was added to a solution of SnCl₄•5H₂O (4 mmol) that had been acidified with H₂SO₄ (6 mL, 0.9 M), resulting in an immediate color change. The obtained compound was then mixed with Ar-C₃N₄/NFT (310 mg) in 9 mL of distilled water and sonicated for 72 minutes. The resulting mixture was stirred at room temperature for 8 hours, after which the solid product was isolated. The material was washed with

dimethylformamide and dried at 85 °C to yield the final Dy₂Sn₂O₇@Ar-C₃N₄/NFT composite.

2-6- Method for the oxidation of sulfur compounds

The reaction mixture contained a sulfur compound in an amount of 0.5 mmol in 5 mL of water. This mixture was subjected to an oxygen pressure of 2 atmospheres, which was introduced into the system at a flow rate of 14 mL/min. In addition, this reaction mixture contained 7 mg of Dy2Sn2O7@Ar-C3N4/NFT nanoparticles, and the system was exposed to UV irradiation (using a 125 W mercury lamp) for a certain period of time. After the reaction was completed, the catalyst was separated from the reaction mixture and purified using ethanol to ensure its reusability in future reactions.

3- Results

3-1- Analysis and discussion of FTIR spectra

Figure 2 shows the Fourier transform infrared (FT-IR) spectra of different cases. In the case of C3N4, a broad signal was observed in the range of 3290 to 2700 cm-1. This signal was associated with the resonance of the H-N bond present in -NH- and H2N-. The presence of these signals indicated the presence of unconjugated amine groups on the surface. In addition, C3N4 showed a specific stretching vibration between 1570 and 1290 cm/s, which was related to the heterocyclic heptazine ring, confirming the formation of triazine. The absorption bands at 800 and 875 cm/s were related to the distortion of the triazine ring and the N-H vibration of C3N4, respectively. In general, Dy2Sn2O7@C3N4/NFT and Ar- C3N4 showed similar FT-IR spectra to C3N4. X-ray diffraction and Fourier transform infrared spectroscopy revealed that the structural integrity of Ar- C3N4 (including its crystal structure and chemical composition) did not change after incorporation into the aromatic component of C3N4. Maintaining the structural integrity of Ar-C3N4 was a beneficial feature that significantly enhanced its photocatalytic capacity.

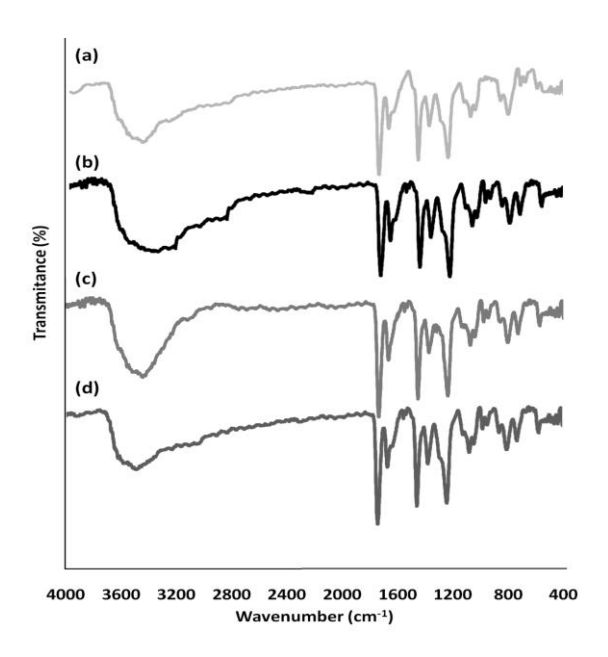


Figure 2- FT-IR spectra of Dy2Sn2O7@C3N4/NFT (a), Dy2Sn2O7@Py-C3N4/NFT (b), Dy2Sn2O7@Pm-C3N4/NFT (c), and Dy2Sn2O7@Ph-C3N4/NFT (d).

3-2- Analysis and discussion of XRD patterns

Figure 3 shows the X-ray diffraction (XRD) patterns of the various cases investigated in this study. All the diffraction peaks were completely consistent with Dy2Sn2O7. It is worth noting that the Dy2Sn2O7@Ar-C3N4/NFT samples showed similar XRD patterns to Dy2Sn2O7@C3N4/NFT. This indicates that the crystal anatomy of the Ar-C3N4 samples remained stable and the amount of Ar contamination was low. In addition, both Dy2Sn2O7 and Dy2Sn2O7@C3N4/NFT showed similar XRD patterns, indicating a uniform distribution of Dy2Sn2O7 species on the outer surface of the lightly loaded Dy2Sn2O7@C3N4/NFT.

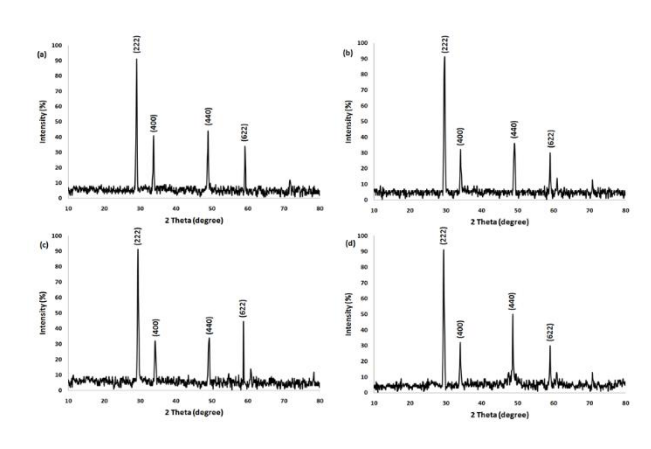


Figure 3- XRD patterns of Dy2Sn2O7@C3N4/NFT (a), Dy2Sn2O7@Py-C3N4/NFT (b), Dy2Sn2O7@Pm-C3N4/NFT (c), and Dy2Sn2O7@Ph-C3N4/NFT (d).

3-3- Analysis and discussion of TEM patterns

Figure 4 shows transmission electron microscopy (TEM) images of Dy2Sn2O7@C3N4/NFT, Dy2Sn2O7@Py-C3N4/NFT, Dy2Sn2O7@Pm-C3N4/NFT Dy2Sn2O7@Ph-C3N4/NFT. The NFT sample showed similar tendencies to barriers with specific dimensions and shapes, with branched molecular fibers ranging in width from 35 to 40 nm. The fibers were arranged in a three-dimensional manner, forming barriers that facilitated unhindered access to the outer layer. The Dy2Sn2O7 nanoparticles attached to the NFT wall and with diameters ranging from 18 to 23 nm showed minimal aggregation. TEM images showed that the number of Dy2Sn2O7 nanoparticles on NFT in the Dy2Sn2O7@Ph-C3N4/NFT sample was significantly than that of Dy2Sn2O7@C3N4/NFT, Dy2Sn2O7@Py-C3N4/NFT and Dy2Sn2O7@Pm-C3N4/NFT. This difference can be attributed to the Ar-C3N4 structure on the NFT surface, which acted as a stabilizing base for Dy2Sn2O7 nanoparticles.

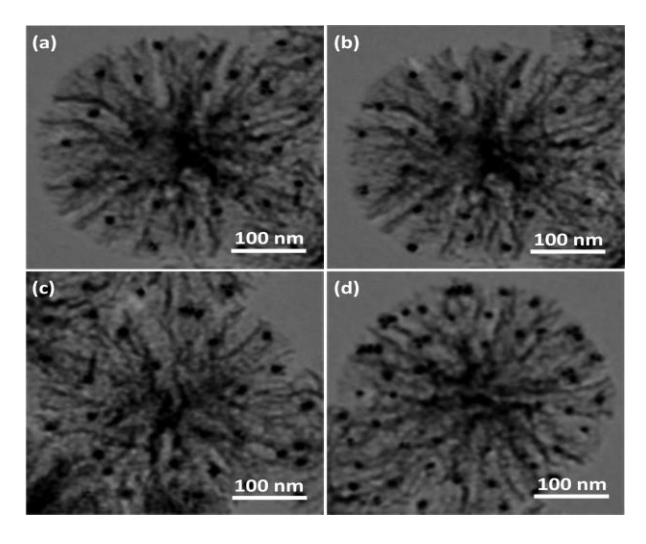


Figure 4- TEM images of Dy2Sn2O7@C3N4/NFT (a), Dy2Sn2O7@Py-C3N4/NFT (b), Dy2Sn2O7@Pm-C3N4/NFT (c), and Dy2Sn2O7@Ph-C3N4/NFT (d).

3-4- Investigation of the Ultra-Accelerated Oxidative Desulfurization (UAOD) Process

The ultra-accelerated oxidation desulfurization (UAOD) method was used in a simulated gasoline oxidation experiment to compare different catalysts. The desulfurization process, which aimed to remove sulfur from gasoline, was carried out for Dy2Sn2O7@Ph-C3N4/NFT, Dy2Sn2O7/NFT, NFT, Dy2Sn2O7, and Ph-C3N4 samples under similar experimental conditions. The results showed that Dy2Sn2O7@Ph-C3N4/NFT, as

a heterogeneous catalyst, exhibited the highest oxidation efficiency among all the evaluated catalysts. Furthermore, the effect of Dy2Sn2O7/NFT was compared with Dy2Sn2O7@Ph-C3N4/NFT under ideal experimental conditions (without the presence of Ph-C3N4). The impressive conversion rate of 99% indicated that the presence of Ph-C3N4 significantly enhanced the oxidation process. The efficiency of the activated silica gel was investigated by showing the relatively low oxidation capacity of Ph-C3N4, which was only 9%. In order to evaluate the effect of the presence of the catalyst, control experiments were carried out in the absence of any catalyst and a conversion rate of only 2% was observed. According to the findings presented in Table 1, it was concluded that Dy2Sn2O7@Ph-C3N4/NFT had the highest catalytic activity and this catalyst was selected to fine-tune several other factors such as catalyst amount, oxygen pressure, reaction time, thermal conditions and PTA allocation.

Table 1- Effect of catalyst on DBT desulfurization

Entry	Catalyst	Conversion
		(%)
1	Dy ₂ Sn ₂ O ₇ @Ph-	99
	C_3N_4/NFT	
2	$Dy_2Sn_2O_7/NFT$	91
3	NFT	26
4	Dy ₂ Sn ₂ O ₇	47
5	Ph-C ₃ N ₄	9
6	-	2

3-5- Influence of Temperature on the Efficiency of DBT Desulfurization

The effect of temperature on the desulfurization process of DBT, which was used as a model fuel, was investigated. The temperature range was from 30 to 70 °C, and a detailed analysis revealed that the optimum temperature for this process was 50 °C. During the experiments, it was found that increasing the reaction temperature to 50 °C resulted in a significant increase in the desulfurization efficiency, reaching 99% efficiency after only 10 min (Figure 5). Surprisingly, further increase in temperature did not lead to further improvement in the conversion rate. This result remained consistent when other model compounds were also

subjected to desulfurization. In addition, the study investigated the effect of different amounts of Dy2Sn2O7@Ph-C3N4/NFT on DBT desulfurization. The researchers investigated a range of amounts from 2 to 8 mg to determine the optimal catalyst concentration.

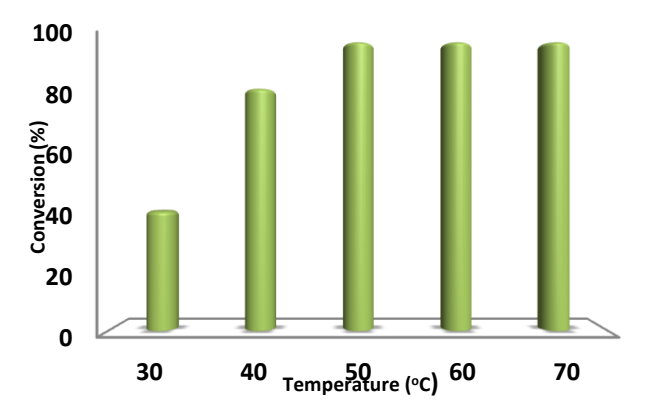


Figure 5- The role of temperature in DBT desulfurization.

3-6- Optimization of Temperature and Catalyst Concentration in the Desulfurization of DBT

The highest conversion rate was obtained when the catalyst concentration was 7 mg, after 10 min at room temperature. Surprisingly, increasing the concentration beyond 7 mg did not lead to a significant improvement in performance. On the other hand, it was observed that using the minimum amount of Dy2Sn2O7@Ph-C3N4/NFT (2 mg) as catalyst resulted in a lower sulfur to sulfone conversion rate of only 22% (as shown in Figure 6). Finally, the results of this study clearly show that there is a complex relationship between temperature and desulfurization efficiency when DBT is used as a model fuel. It was found that the optimum temperature for this process is 50 °C and increasing the temperature beyond this point does not provide any additional benefit. Furthermore, the investigation of the catalyst concentration showed that using a concentration of 7 mg resulted in the highest conversion rate and increasing the concentration further did not lead to any significant improvement. Therefore, these findings provide valuable insights into the design and optimization desulfurization processes and can help improve the efficiency and effectiveness of fuel treatment methods.

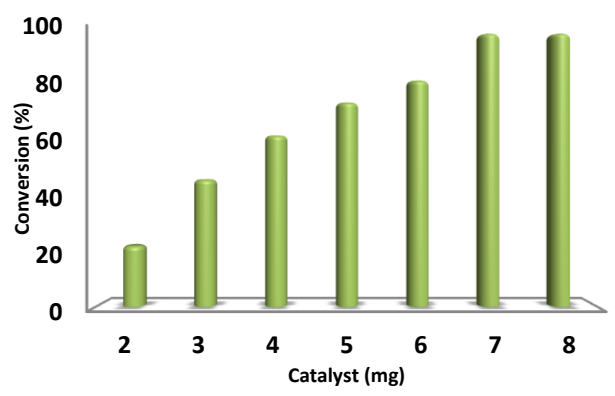


Figure 6- Effect of Dy2Sn2O7@Ph-C3N4/NFT content on DBT desulfurization.

3-7- Effect of Reaction Time on DBT Desulfurization

The results of the reaction time are presented comprehensively in Figure 10, which provides a visual representation of the findings. As the graph clearly shows, the degree of conversion reached 99% after only 10 minutes of reaction time (Figure 7).

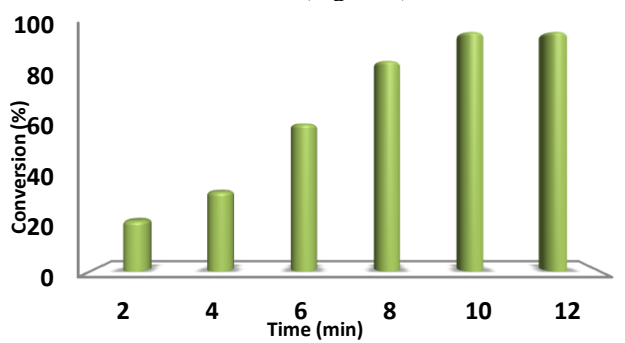


Figure 7- The role of time in DBT desulfurization.

4-Comparison with Other Studies

The results obtained in this investigation regarding the synthesis and application of fibrous nanoceramics for refinery wastewater treatment were compared with those reported by other researchers in related studies. This comparison aims to clarify the research position of the present work within the broader scientific context and to highlight its distinctive strengths and possible limitations. The outcomes demonstrate that the synthesized fibrous nanoceramics exhibit remarkable efficiency in removing specific pollutants commonly present in refinery wastewater, such as petroleum hydrocarbons and heavy metals. These findings are consistent with previous reports [11–13], which likewise emphasized the high adsorption potential of nanoceramic-based materials in the treatment of industrial effluents.

Furthermore. several studies have explored in adsorption technologies advancements and underscored the significance of selecting suitable adsorbents for targeted pollutants [14–17]. In this regard, the current research contributes a practical approach by introducing a tailored fibrous nanoceramic adsorbent specifically designed for refinery-derived contaminants. Recent investigations have also addressed the ability of nanoceramics to remove heavy metals from wastewater. Compared with those studies [18:19]. the present research not only evaluates heavy metal removal but also extends the investigation to the elimination of hydrocarbons and other organic compounds, thereby broadening the scope of application.

Some researchers have highlighted the existing challenges and limitations associated with the use of nanomaterials in water treatment processes [20–22]. This study likewise discusses these issues and offers practical recommendations to minimize potential adverse environmental impacts.

Overall, the findings suggest that fibrous nanoceramics hold strong promise as an efficient and sustainable material for refinery wastewater purification. Nevertheless, further research is recommended to optimize the synthesis parameters, reduce production costs, and thoroughly assess the long-term environmental implications of these materials.

5- Conclusion

Conclusion Novel nanoparticles with the ability to precisely tune the accuracy and efficiency of the sulfur photodesulfurization process were developed through engineering and targeted modification of the catalytic active sites. The research methodology was designed based on the synthesis of the Ar-C₃N₄/NFT system with a fibrous-tree structure, in the presence of Dy₂Sn₂O₇ as a self-assembled template. This process consisted of three key steps: continuous photomodification, chemical annealing, and reduction. In order to identify and evaluate the structural features of the synthesized system, a series of physical and chemical analyses were performed, including mesoporous studies, surface texture, and morphology of the nanoparticles. The synthesized Dy₂Sn₂O₇@Ar-C₃N₄/NFT fibrous-tree nanoparticles showed a significant improvement in photocatalytic performance compared to similar spherical samples. The desulfurization process from natural gasoline was carried out with high efficiency and a conversion rate of 99%. Furthermore, sulfur compounds from mustard gas were completely oxidized to sulfoxide using hydrogen peroxide under ambient conditions, with an impressive selectivity of 100%. This performance enhancement is mainly due to the synergistic effect between Dy₂Sn₂O₇ and Ar-C₃N₄. The prepared catalyst retained more than 97% of its initial activity after ten independent use cycles, thus clearly demonstrating its stability and high potential for reuse.

References

- [1] A.K. Gupta, S.K. Gupta, D. Chauhan, Mater. Chem. Phys., 210 (2018) 475–485.
- [2] J. Liang, Y. He, T. Wang, J. Environ. Eng., 145 (2019) 04019052.
- [3] Y. Zhang, et al., Environ. Sci. Rev., 22 (2024) 26. https://doi.org/10.1186/s12951-023-02151-3.
- [4] G. Palani, et al., Molecules, 26 (2021) 2799. https://doi.org/10.3390/molecules26092799.
- [5] A.G. Niculescu, et al., Polymers, 16 (2024) 709. https://doi.org/10.3390/polym16050709.
- [6] J. Keerti, Molecules, 26 (2021) 1797. https://doi.org/10.3390/molecules26061797.
- [7] M. Nasrollahzadeh, et al., J. Hazard. Mater., 401 (2020) 123401.
- https://doi.org/10.1016/j.jhazmat.2020.123401.
- [8] M. Nasiri, et al., J. Environ. Chem. Eng., 15 (2025) 120198
- [9] M. Omrani, A. Karimi, S.M. Hosseinzadeh, J. Environ. Chem. Eng., 11 (2023) 110012.
- [10] M.A. Mahmoud, S. Sharma, Environ. Int., 146 (2021) 106205.
- [11] Tang, S., et al., Chemosphere, 234 (2019) 658–667.
- [12] Rawool, S. A., et al., Mater. Adv., 3 (2022) 8449–8459.
- [13] Rawool, S. A., et al., ACS Appl. Energy Mater., 3 (2020) 8150–8158.
- [14] Nazeer, A., et al., Environ. Technol. Rev., (2021) 1–16.
- [15] Sahu, O., et al., Water Sci. Technol., 67 (2022) 1589–1602.
- [16] Nematollahi, M., et al., Environ. Eng. Res., 26 (2021) 1861–1873.
- [17] Hashemi, S. Z., et al., Desalination Water Treat., 197 (2020) 42–54.
- [18] Cerozi, B. G., et al., Sustain. Mater. Technol., 27 (2021) e00254.
- [19] Shirodkar, S., et al., Resour. Conserv. Recycl., 168 (2022) 105227.
- [20] Schwartz, E. M., et al., Nat. Sustain., 4 (2021) 123–134.
- [21] Bi, Y., et al., Environ. Pollut., 268 (2021) 115540.
- [22] Petruzzelli, D., et al., Environ. Sci. Ecotechnol., 15 (2022) 200158.